Journal of the Nigerian Mathematical Society
Vol. 41, Issue 3, pp. 261-274, 2022


# ON THE NUMERICAL SOLUTION OF THE KURAMOTO-SIVASHINSKY EQUATION USING OPERATOR-SPLITTING METHOD

A. A. ADEROGBA[1,2], M. CHAPWANYA[1] AND J. K. DJOKO[1]

Abstract. An operator-splitting scheme for the Kuramoto-Sivashinsky equation, $u_t + uu_x + u_{xx} + u_{xxxx} = 0$, is proposed. The method is based on splitting the convective and the diffusive differential terms thereby permitting an efficient scheme choice for each of them, and when combined give a reliable solution for the entire equation. We demonstrate the accuracy and capability of the proposed split scheme via several numerical experiments. In order to further demonstrate the efficiency of the numerical approach, the computations of the bound, $\limsup_{t\to\infty} \|u(x,t)\|_2$ for the equation is presented and shown to be consistent with the earlier obtained analytical result.

Keyword: Kuramoto-Sivashinsky equation; fractional step-splitting; numerical solution; energy bounds.
2010 Mathematical Subject Classification: 65M06; 65M08; 97N40

## 1. Introduction

In this paper we consider the numerical solution of the Kuramoto-Sivashinsky problem

$$\begin{cases} u_t + uu_x + \alpha u_{xx} + \gamma u_{xxxx} = 0, \quad \forall\ (x,t) \in \mathbb{R} \times (0,\infty), \\ u(x,0) = \psi(x), \end{cases} \tag{1.1}$$

where the subscripts denote derivatives with respect to the indicated variables, and $\alpha, \gamma > 0$ are constant coefficients accounting for the long wave instability (gain) and short wave dissipation, respectively. Equation (1.1) is a well-known model of one dimensional turbulence which was derived in various physical contexts including chemical-reaction waves, propagation of combustion fronts in gas, surface waves in a

Received by the editors February 14, 2022; Revised: October 17, 2022; Accepted: November 02, 2022
www.nigerianmathematicalsociety.org; Journal available online at https://ojs.ictp.it/jnms/

film of a viscous liquid flowing along an inclined plane, patterns in thermal convection, rapid solidification, and many others (see for example [1, 2, 3, 4, 5, 6]).

Several results have been reported in the literature on the properties of the solution of the Kuramoto-Sivashinsky (K-S) equation, with special attention on the energy

$$\mathcal{E}(t) = \frac{1}{L}\int_0^L u^2 dx, \tag{1.2}$$

which has been derived theoretically in the form of the bound

$$\limsup_{t\to\infty} \|u(x,t)\|_2 = \limsup_{t\to\infty} (L\mathcal{E}(t))^{1/2} \leq CL^p. \tag{1.3}$$

For example, [7] determined $p$ to be $5/2$ with the assumption that initial data is L-periodic, antisymmetric about the origin and of zero mean. In [8], the authors removed the antisymmetry requirement and observed that $p$ is $8/5$. In [9], a 1-dimension version of the equation was considered without the requirement of odd solutions and arrived at the same value of $p$ following a generalization of Lyapunov function argument from [7] . Following a $div - curl\ argument$, [10] obtained $p = 3/2$. A weaker bound which was proved to be necessary in the presence of a linear destabilizing term was later introduced in [11]. Recently, [12] followed a Lyapunov argument to obtain bounds that are independent of the system size. Global existence result was recently given for a $2-$dimensional Kuramoto-Sivashinsky model in [13].

The numerical solutions of the K-S equation have been widely investigated in the literature. In particular, we highlight the Galerkin method [14], the Chebyshev spectral methods [15], the B-splines [16], the meshless method of lines [17], etc. The aim of these investigations have been on the accuracy [14], and/or how these solutions compare with the well-documented benchmark solutions [18]. In [14], an explicit Runge-Kutta method was used to avoid the restrictive stability limit of the fourth order derivative. Further advantage of the method is that the approach can easily be tweaked to obtain any required order of accuracy. Other approaches are based on simplifying the partial differential equation so that it can be handled easily by a computer. For example, the B-spline approach by [16] reduced the problem to a set of algebraic equations, while in [15], the equation was reduced to a system of ODEs that were solved by implicit-explicit BDF methods.

The fractional splitting method which originates from the respective novel works of [19, 20] and [21] on Alternating Directional Implicit (ADI) and Local One Dimensional (LOD) methods is employed in this article. In this paper we use the fractional splitting/step method which originated from the work of [19, 20] on Alternating Direction Implicit (ADI) method and local-one-dimensional (LOD) method proposed later in [21]. This method allows a complex differential equation to be split into different subproblems based on different sub-operators/physical models present in the original equation. Each of these sub-equations are solved by best available method. The Kuramoto-Sivashinsky equation (1.1) consists of two different spatial operators: the linear and the nonlinear operators. Interestingly, the nonlinear operator is hyperbolic, i.e., it is known to introduce discontinuity in finite term while the linear term has a stabilizing effect. Consequently, the equation is split into two physical processes evident in the equation: the convection (inviscid Burgers) equation and the linear fourth order equation

$$u_t + uu_x = 0, \quad \forall (x,t) \in \mathbb{R}\times(0,\infty), \tag{1.4}$$

and

$$u_t + \alpha u_{xx} + \gamma u_{xxxx} = 0, \quad \forall (x,t) \in \mathbb{R}\times(0,\infty). \tag{1.5}$$

From an abstract point of view, the space discretized problem is a system of ordinary differential equations and can be written as

$$\frac{du}{dt} + L(u) + N(u) = 0, \tag{1.6}$$

with initial condition $u(0) = u^0$, where $N$ is the discretization of the nonlinear (convection) operator and $L$ is the discretization of the linear operator. Assuming the solution $v^n \approx u(t_n)$, has been computed, then the next approximation is found from the fractional steps

$$\frac{du^*}{dt} + N(u^*) = 0, \quad u^*(t_n) = v^n, \tag{1.7}$$

$$\frac{du^{**}}{dt} + L(u^{**}) = 0, \quad u^{**}(t_n) = u^*(t^{n+1}), \tag{1.8}$$

and set $v^{n+1} = u^{**}(t^{n+1})$. The solution $u^*$ of the non linear equation becomes an intermediate solution of the equation while $u^{**}$ gives rise to the approximation of the entire equation after the completion of the integration. For the time integration, the nonlinear convection equation makes use of implicit and total variation diminishing (TVD) schemes, while scheme designed for stiff problems are used for the linear term.

This work aims to present a reliable solution approach and numerically validate some of the theoretical results of the K-S equation documented in the literature. We verify the results stated above on the bound of the solution and the preservation of the periodicity and zero average as observed in [10]. The plan of this article is as follows: In Section 2, we give comprehensive outline on the numerical schemes employed, while in Section 3 the convergence of the schemes, the stability of the traveling wave solution and the chaotic nature of the solution are validated. We end the section by discussing the properties of the solution including a computation of the bounds introduced in earlier work.

## 2. Numerical Schemes

The notation adopted here is consistent with those known in the finite volume discretization literature, see for example [22]. A uniform mesh, $x_{i+1/2}$ with fixed width $\Delta x$, where $x_i = ih$, $i = 0, 1, 2, \cdots, m$ is considered. The uniform time mesh is also employed, i.e., $t^n = n\Delta t$, $n = 0, 1, 2, \cdots$, with fixed time step size $\Delta t > 0$. To take into account the discontinuity which may arise due to the convection equation in finite time, we employ the finite volume approach so that $v_i^n$ is considered as the approximation to the cell average of the true solution, thus,

$$v_i^n = \frac{1}{\Delta x} \int_{x_{i-1/2}}^{x_{i+1/2}} u(x, t_n) dx.$$

**Remark 1.** [10] *discussed the effect of the nonlinear convection term and the linear term on the solution of the K-S equation. Their theoretical arguments were established via the operator splitting method. Our choice of shock capturing schemes for our numerical approximation is to remove every doubt of nonphysical oscillation that may arise during the simulation. We will be able to verify our simulation with their theoretical results.*

**Remark 2.** *Most of the convection term solvers compared here are first order schemes (for comparison). Being first order will reduce the total order of the scheme to one after the splitting procedure.*

2.1. **The convection term.** The convection term is the hyperbolic (inviscid Burgers) equation. In conservative form, it can be written as

$$u_t + f(u)_x = 0, \tag{2.1}$$

where $f(u) = u^2/2$; which is a widely studied partial differential equation and occurs in various areas of applied mathematics. It has the main property of developing shocks (discontinuities) in finite time. We employ second order, TVD schemes and some implicit schemes with a general conservative representation

$$v_i^{n+1} = v_i^n - \lambda(F_{i+1/2} - F_{i-1/2}), \tag{2.2}$$

where $\lambda = \frac{\Delta t}{\Delta x}$ is the Courant-Friedrichs-Lewy (CFL ) number and $F_{i+1/2}$ is a numerical flux which gives the intercell average flux at the interface $x_{i+1/2}$. The approximation of $F_{i+1/2}$ leads to different types of finite volume schemes for equation (2.1). For the sake of completeness, we list below the schemes for equation (2.1) below.

The *implicit schemes* are derived with the numerical flux approximated as

$$F_{i+\frac{1}{2}} \simeq \frac{1}{2}[(1-\theta)(f(v_i^n) + f(v_{i+1}^n)) + \theta(f(v_i^{n+1}) + f(v_{i+1}^{n+1}))],$$

and is fully implicit (FUIM) scheme when $\theta = 1$ or Crank-Nicolson scheme (CNS) when $\theta = 0.5$.

The *Godunov scheme* assumes a numerical flux

$$F_{i+\frac{1}{2}} \simeq f(v_i^n) + \frac{\Delta x}{2} f'(v_i^n)\left[1 - f'(v_i^n)\lambda\right]\sigma_i^n,$$

where $\sigma_i^n$ is a slope limiter.

The *non staggered central difference (NSTG) scheme* is a second order extension of the non staggered version of the central difference scheme by Lax-Friedrich (see for example [23], [24]) with a numerical flux

$$F_{i+\frac{1}{2}} = -\frac{1}{4}\left[v_{i+1}^{'n} + 2\lambda f(v_{i+1}^{n+1/2})\right], \tag{2.3}$$

where

$$v_i^{n+1/2} = v_i^n - \frac{\lambda f_i'}{2}. \tag{2.4}$$

Furthermore, the non oscillatory behavior of this second order scheme is guaranteed by the choice

$$v_i' = \text{minmod}\left(\Delta v_{i+1/2}, \Delta v_{i-1/2}\right),$$

and

$$f_i' = a(v_i)v_i',$$

where $a(v_i)$ is the derivative of the flux function with respect to the argument $v_i$ which should be interpreted as the Jacobian when dealing with systems of conservation laws.

The second order *semi-discrete central (SemiD) difference scheme* (see [25], [24], [26]) in the conservative form employs a numerical flux

$$F_{i+1/2} = \frac{f(v_{i+1/2}^+) + f(v_{i+1/2}^-)}{2} - \frac{a_{i+1/2}}{2}(v_{i+1/2}^+ - v_{i+1/2}^-), \tag{2.5}$$

where the intermediate values $v_{i+1/2}^{\pm}$ are given by

$$v_{i+1/2}^+ = v_{i+1} - \frac{\Delta x}{2}(u_x)_{i+1}, \quad v_{i+1/2}^- = v_i + \frac{\Delta x}{2}(u_x)_i, \tag{2.6}$$

and the maximal local speed $a_{i+1/2}$, in the scalar case with convex flux, is given as

$$a_{i+1/2} = \max(|f'(v_{i+1/2}^-)|, |f'(v_{i+1/2}^+)|).$$

Also, the slope $(u_x)_i$ is given by the minmod function

$$(u_x)_i = \text{minmod}\left(\frac{v_{i+1}-v_i}{\Delta x}, \frac{v_i - v_{i-1}}{\Delta x}\right).$$

**Remark 3.** *Throughout this paper, we choose the CFL number to be less than* 1*, which is within the stability requirement of all the schemes considered.*

Here we present a test example to support the choice of schemes for the convection subproblem. In particular, it is known, that the solution of the advection problem preserves the average energy density until the formation of the shock [10].

**Example 1.** *We consider*

$$\begin{cases} u_t + uu_x = 0, \ \forall\ (x,t) \in (0,L)\times\mathbb{R}, \\ u(0,x) = 0.5 + \sin(x)\,, \\ u(t,x) = u(t,x+L). \end{cases} \tag{2.7}$$

The profiles of $E(u(t))$ in Fig. 1 show the conservation of $E(u(t))$ before the development of shock. This is a generic behaviour of the solution of hyperbolic equations. The work [10] claimed that the convection term preserves the mean energy density before the onset of shock. This is confirmed by all the schemes through Fig. 1. These profiles also show that the shock develops at about time $T = 1$ except for the Godunov scheme. The semi-discrete central and the implicit schemes agreed with the approximation of time of shock development while the non-staggered central scheme depict shock as setting in a little earlier before $T = 1$. These all agree with the assertion by [25]. The down-hill sawtooth behaviour of the mean energy after the shock in the implicit schemes (which is more pronounced in the Crank-Nicolson scheme) may be due to oscillation about the shock region as observed in the earlier work of [27].

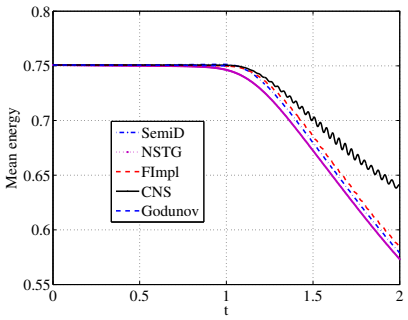


FIGURE 1. Mean energy density profiles for problem (2.7).

2.2. **The linear terms.** In this section, we consider three different schemes to be compared for the numerical solutions of the linear subproblem (1.5) with $\alpha = \gamma = 1$. Via the $\theta$-scheme, we consider the implicit schemes in the following form

$$v_i^{n+1} + \theta f_i^{n+1} = v_i^n - (1-\theta) f_i^n, \quad i = 1, 2, \cdots, m-1, \tag{2.8}$$

where

$$f_i^n = r(v_{i-1}^n - 2v_i^n + v_{i+1}^n) + \mu(v_{i-2}^n - 4v_{i-1}^n + 6v_i^n - 4v_{i+1}^n + v_{i+2}^n),$$

$\mu = \alpha\frac{\Delta t}{\Delta x^4}$, and $r = \gamma\frac{\Delta t}{(\Delta x)^2}$. The scheme is fully implicit if $\theta = 1$ and Crank-Nicolson (C-N) if $\theta = 0.5$. We have chosen to ignore the explicit scheme $\theta = 0$ because of its

restrictive stability condition which requires a time step of $\mathcal{O}((\Delta x)^4)$. This scheme obviously requires some ghost points which are eliminated through the boundary conditions. Next, the backward differentiation formula (BDF2) is considered in the form

$$3v_i^n + 2f_i^n = 4v_i^{n-1} - v_i^{n-2}, \quad n \geq 2, \tag{2.9}$$

where for $n = 1$ we apply the backward Euler scheme

$$v_i^n = v_i^{n-1} + f_i^n,$$

with $f_i^n$ as given above. To serve as a benchmark for other schemes, we also consider the spectral method. Here, the MATLAB in-built fast Fourier transform is employed to solve the equation.

For finite domains, the boundary conditions are either periodic or non periodic in which for the non-periodic case we have nonhomogeneous Dirichlet and Neumann boundary conditions as follows:

$$u(0,t) = g(0,t), \quad u_x(0,t) = g_x(0,t), \quad u(L,t) = g(L,t), \quad u_x(L,t) = g_x(L,t),$$

on both ends where $g(x,t)$ is the exact solution. In particular, we introduce ghost, $v_{-1}$ and $v_{m+1}$, points which are eliminated via approximate boundary values using the following discretization,

$$v_0^n = g_0^n, \quad \frac{-3v_{-1}^n + 4v_0^n - v_1^n}{2\Delta x} + O(\Delta x^2) = g_x(0,t), \tag{2.10}$$

and

$$v_m^n = g_m^n, \quad \frac{v_{m-1}^n - 4v_m^n + 3v_{m+1}^n}{2\Delta x} + O(\Delta x^2) = g_x(L,t) \tag{2.11}$$

respectively.

As a test problem, we present simulations for the growth of energy density. It is claimed, see for example [10], that the energy density for the diffusion problem grows exponentially.

**Example 2.** *We consider*

$$\begin{cases} u_t + u_{xx} + u_{xxxx} = 0, \ \forall\ (x,t) \in (0,L) \times \mathbb{R}, \\ u(x,0) = \exp(-x^2), \\ u(t,x) = u(t,x+L). \end{cases} \tag{2.12}$$

The growth of the mean energy of the diffusion equation as shown in Fig. 2 agrees with the earlier observations (see [10] and the references therein). In Table 1 we also present $L^\infty$ error calculations when the initial condition is changed to $u(x,0) = \sin(x)$ – which is also the exact solution to the linear equation.

From here forthwith, the convection term is solved by any of the above mentioned schemes while the diffusion term is solved by the spectral method when dealing with periodic boundary conditions and BDF2 when dealing with non periodic boundary conditions. The C-N scheme was dropped because of computational cost. Hence, we will refer to the method of solution of the K-S equation by the scheme used to handle the convection term. In all the schemes we will choose 320 grid points.

## 3. Numerical Experiments

In this section, we consider the computational domain to be $[-30, 30]$ with a focus to compute the solution of the entire K-S equation using the fractional time step method described in Section 2. We test the convergence of the proposed scheme via a test problem where the exact solution is known [14].

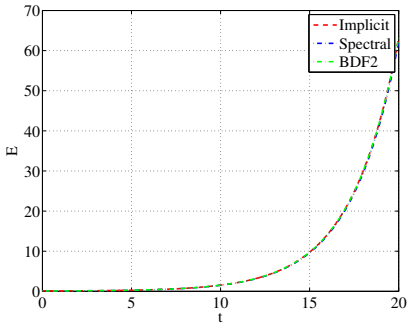


FIGURE 2. Mean energy density profile for the diffusion term.

| Grid points | $L^\infty$ error $\times 10^4$ at T = 1 | | |
|---|---|---|---|
| | CNS | Spectral | BDF2 |
| 20 | 74.4087 | 1516.61 | 74.4253 |
| 40 | 19.1106 | 773.780 | 19.1108 |
| 80 | 5.02760 | 390.024 | 5.02761 |
| 160 | 1.28539 | 195.709 | 1.28539 |

TABLE 1. Error due to each scheme for the numerical approximation of the linear equation.

**Example 3.** *Consider*

$$\begin{cases} u_t + uu_x + u_{xx} + u_{xxxx} = 0, \quad x \in (-L, L), \quad t > 0 \\ u(x,0) = g(x,0), \\ u(-L,t) = g(-L,t), \quad u(30,t) = g(L,t), \\ u_x(-L,t) = g_x(-L,t), \quad u_x(L,t) = g_x(L,t), \end{cases} \tag{3.1}$$

where $g(x,t)$ is the exact solution given by

$$g(x,t) = c + \frac{15}{19}\sqrt{\frac{11}{19}}(-9\tanh[l(x-ct-x_0)] + 11\tanh^3[l(x-ct-x_0)]).$$

The ghost points are taken care of via equations (2.10) and (2.11). In the simulations, we take $x_0 = -12$, $c = 5$, and $l = \frac{1}{2}\sqrt{\frac{11}{19}}$ as documented in [14, 28].

The profiles of the solution generated by the different schemes in comparison with the exact solution including the close peaks are shown in Fig. 3. The deviation of all the numerical schemes from the exact solution is shown in Fig. 3(a) while Fig. 3(b) reveals the deviation of each of the schemes at the highest peak. Of particular interest, the NSTG scheme gives the largest deviation from the exact solution at the peak.

From Table 2, when the initial data that corresponds to the exact solution of the K-S equation was employed, the explicit schemes behaves far better than the implicit ones. The semi-discrete is consistent in producing the least possible error out of the explicit schemes. It is also evident that the non-staggered central scheme is better than any of the other schemes.

3.1. **The traveling wave solution.** The traveling wave solution of every time-dependent partial differential equation gives the solution at all times. Therefore to

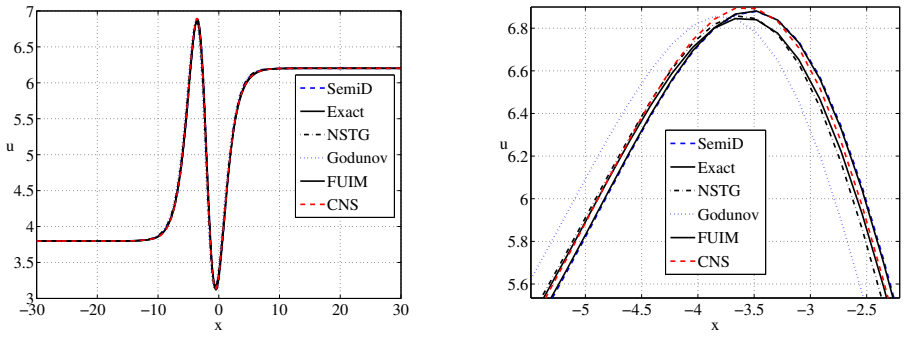


(a) All schemes with the exact solution. (b) Close-up near the maximum.

FIGURE 3. Comparison of the exact solution with the numerical solutions.

| Grid points | $L_\infty$ error (convergence rate, $p$) at T = 1 | | | | |
|---|---|---|---|---|---|
| | Godunov | Semi-Discrete | Non-staggered | CNS | Fully Implicit |
| 40 | 1.040 | 1.373 | 1.883 | 1.588 | 1.608 |
| 80 | 1.512 (-0.54) | 0.535 (1.36) | 1.258 (0.58) | 0.709 (1.16) | 0.688 (1.22) |
| 160 | 0.950 (0.67) | 0.137 (1.97) | 0.6011 (1.07) | 0.206 (1.78) | 0.222 (1.63) |
| 320 | 0.268 (1.82) | 0.178 (2.94) | 0.2197 (1.45) | 0.056 (1.88) | 0.068 (1.71) |
| 640 | 0.099 (1.43) | 0.007 (1.41) | 0.0698 (1.65) | 0.021 (1.45) | 0.028 (1.26) |

TABLE 2. Convergence rate of the fractional step for the K-S equation with initial data that corresponds to the exact solution.

test the accuracy of the numerical schemes, it makes sense to initialize the solution with the traveling wave solution and check the deviation of the schemes from the traveling wave solution as time advances, [27]. This is advantageous over any other solution since the chaotic behavior of (3.4) is restricted to it being integrated over a finite $x-$domain with periodic boundary conditions. Therefore, following the work of [29, 27] (and references therein), we use the transformation $u(x,t) = u(z)$ where $z = x - st$, $s$ is the wave speed, so that the traveling wave solution is defined over the entire $z-$domain, $-\infty < z < +\infty$. The boundary conditions are such that $u \to u_l$ as $z \to -\infty$ and $u \to u_r$ as $z \to +\infty$. The substitution above reduces equation (3.4) to an ordinary differential equation which can be integrated once to give

$$u''' = c + su - \frac{1}{2}u^2 - u', \tag{3.2}$$

where the prime denotes the derivative with respect to $z$. The wave speed $s$ and the constant of integration $c$ are determined by the far field solutions as

$$s = \frac{u_l + u_r}{2}, \quad c = -\frac{u_l u_r}{2}.$$

The wave speed is found via the Rankine-Hugoniot condition to be

$$s = \frac{f(u_r) - f(u_l)}{u_r - u_l}.$$

The spatiotemporal behavior of the solution of (3.2) had been recorded by many authors (see [10, 29, 30, 31] among many). In [30], they gave the steady solution of

(3.1) and studied the solution as a function of the square of a parameter $c$. With this, he classified the behavior of the solution as conical (for large value of $c^2$), periodic or quasi-periodic (for small values of $c^2$). Later, [29] classified the solution based on the shock development as either regular shocks, solitary waves or oscillatory shocks. This they did by observing the far field behavior of the solution. They also noted that experiments may show chaotic behavior with respect to traveling waves. Recently, [31] employed the conditions for solitary and periodic waves to derive an exact solution to the traveling wave. Here we implement the oscillatory shock behavior as given in [29]. Thus, we solve the non homogeneous ordinary differential equation

$$\begin{cases} u''' + u' - (s + 0.5s)u = c, \\ u \to u_l \quad as \quad z \to -\infty, \\ u \to u_r \quad as \quad z \to \infty. \end{cases} \tag{3.3}$$

In addition, we ensure the first derivatives vanish at both ends. The nonlinear boundary value problem (3.3) was discretized and the system of equations derived were solved by the Newton's method. We highlight here that our numerical approach was able to reproduce most of the different families of solutions predicted in [29]. For the oscillatory shock considered here, we impose the far field boundary values, $u_l = 1 = -u_r$, consistent with the work of [29].

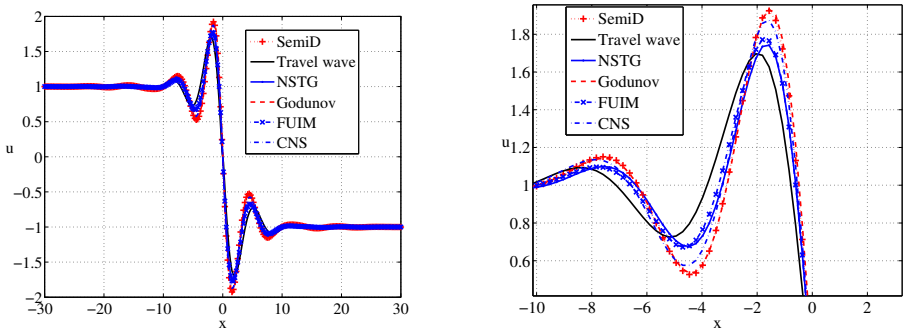


(a) All schemes with the traveling wave. (b) Close-up near the maximum.

FIGURE 4. Traveling wave solution as standard compared to other schemes at $T = 10$.

The results in Fig. 4 were all generated as outlined above. We highlight that all the schemes produced the same quantitative behavior. Nevertheless, NSTG and the fully implicit scheme solution are the closest to the traveling wave solution with the NSTG giving the least deviation from the traveling wave solution. The Godunov and the semi-discrete scheme solutions (overlap) gave the largest deviation of all the schemes.

**Note 1.** *Considering the relatively poor performance of the Godunov scheme's mean ennergy approximation of the Burger's equation* (2.7) *as well as the error and convergence rate on approximating the K-S equation* (3.1) *as shown in Table 1 as compared to others, henceforth, we will drop its usage.*

3.2. **The chaotic property.** In this section we show the capability of the designed scheme to produce chaotic solutions associated with the K-S equation.

**Example 4.** *We consider*

$$\begin{cases} u_t + uu_x + u_{xx} + u_{xxxx} = 0, \quad x \in (-L, L), \quad t > 0 \\ u(x,0) = \exp(-x^2), \\ u(x,t) = u(x+L,t), \end{cases} \tag{3.4}$$

*with* $L = 15$.

We can see that the numerical simulations in Fig. 5 are consistent with the work [14]. We highlight the convergence of the presented scheme from the computations of Fig. 5(a) and Fig. 5(c). In particular, the grid refinement from 160 to 320 grid points assert this.

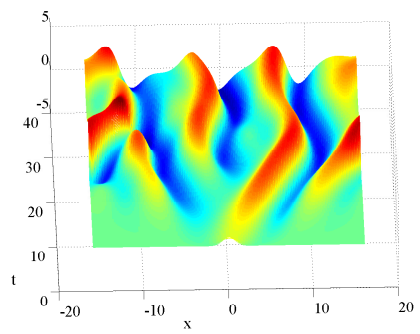


(a) Surface plot on 160 grids

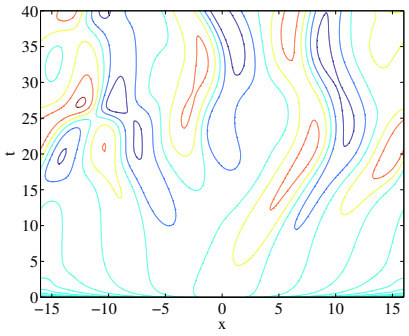


(b) Contour plot showing the peaks on 160 grids

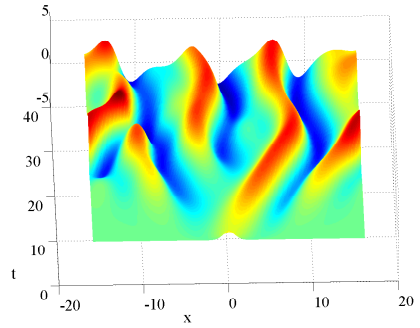


(c) Surface plot on 320 grids

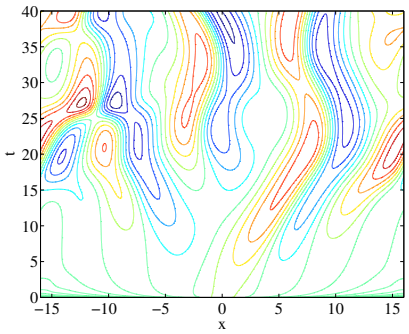


(d) Contour plot showing the peaks on 320 grids

FIGURE 5. The chaotic solution of the K-S equation with Gaussian initial conditions up to $T = 40$.

3.3. **The mean energy bound.** We begin this section by validating the bound for the mean energy density of the full K-S equation. In particular, [10] claimed that the effect of (2.7) will balance the exponential growth of (2.12) resulting in a bound for the mean energy of the entire K-S equation. For the numerical experiment we formulate the problem as follows

**Example 5.** *Consider*

$$\begin{cases} u_t + uu_x + u_{xx} + u_{xxxx} = 0, \quad \forall\ (x,t) \in (0,L) \times \mathbb{R}, \\ u(0,x) = \exp(-x^2)\,, \\ u(t,x) = u(t,x+L). \end{cases} \tag{3.5}$$

The validation is given in Fig. 6. We note that all the schemes determine approximately the same bound. However the non-staggered scheme gives a profile lower that the other schemes.

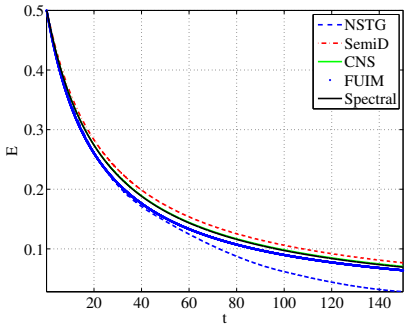


FIGURE 6. Mean energy profiles for the full K-S equation.

Next, we validate the bound as proved in earlier literatures. We write the inequality (1.3) above as

$$\limsup_{t\to\infty} \|u\|_2 = \left(\int_0^L u^2 dx\right)^{\frac{1}{2}} = \mathcal{O}(L^p). \tag{3.6}$$

Here, $p$ is the exponent of $L$ in each of the inequalities. Hence, we plot $\log(\|u(x,t)\|_2)$ against $\log(L)$ and the slope of the graph gives the value of $p$. This we show in the figures below for each of the fractional splitting schemes and the spectral method. The conjectured bound is of $\mathcal{O}(L)$ (see [32] and literatures therein). The value of the slope of each of the graphs in Fig. 7a agrees with this claim.

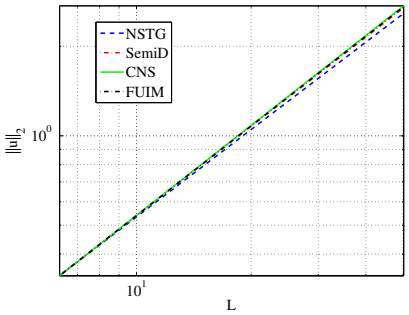


(a) Bound of (3.6)

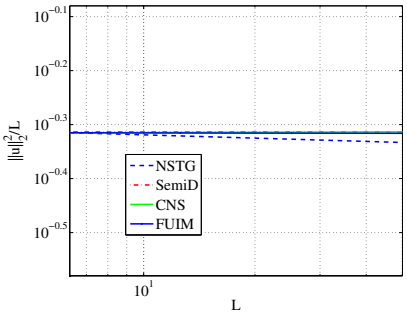


(b) Bound on (3.7)

FIGURE 7. (a) Loglog plot of the $\|u\|_2$. (b) Loglog plot of $\frac{\|u_x\|_2^2}{L}$.

It is obvious that the value of p (0.976659) given by NSTG scheme is lower than the rest. For the Fully implicit scheme $p = 1.00469$, for the C-N scheme $p = 1.0074$, for semi-discrete scheme $p = 0.998822$. Fig. 7b shows the system size independence of the quantity

$$\|u_x\|_2^2 = \int_0^L u_x^2 dx, \tag{3.7}$$

as proved theoretically in [12]. Hence, the expression in (3.7) should be of $\mathcal{O}(L^0)$. Our computation reveals that the exponent is $-0.0202529$, $0.000108553$, $0.006311$ and $0.000948$ for the NSTG, semi discrete, fully implicit and C-N schemes respectively. It is also evident from the Fig. 7b that NSTG deviates much from all other schemes. It is obvious from the Figure that the semi-discrete and the implicit schemes behave equally well unlike the non staggered central scheme.

## 4. Conclusions

In this paper we validated the bounds of the solution to the K-S equation as documented in the literature and several properties mentioned in Section 2 using the fractional time-splitting method. We used several numerical examples to highlight the capabilities of the method. For the Burger's equation, we showed that our selected schemes conserve energy before the onset of the shock while the energy density grows exponentially for the linear terms. When the fractional time-splitting scheme is implemented, we showed that the mean energy of the full scheme is bounded.

The results presented allow us to point at the efficiency, accuracy and stability of the presented schemes. In particular, all the schemes required less than 60 seconds of computer time on a 2.50 GHz Windows PC with 2.0GB of RAM. In summary, the NSTG scheme performed better than all the other schemes considered in this work. This can be seen in Table 2 and backed by comparison of the schemes to the exact solution as given in Fig. 3(b).

On the validation of the zero average, the implicit schemes perform better than the explicit schemes. The little deviations of up to $\pm 10^{-3}$ from zero are observed for the explicit schemes. Considering the dependence of the $\mathcal{L}_2$ norm of the solution on the system size and system size independence of the quantity

$$\frac{\|u_x\|_2^2}{L},$$

the implicit and the semi-discrete schemes perform better than the NSTG.

In this article, we have employed first order schemes for our simulations. It is possible to improve both the spatial and temporal order of accuracy of the simulation in this article. Very soon, we will present results towards this by employing both standard and non standard methods for spatial discretization while exponential time differencing coupled with Runge-Kutta will be used for temporal integration. This method will also be used in simulating the fractional Kuramoto-Sivashinsky model proposed and approximated in [33].

## References

[1] Y. Kuramoto and T. Tsuzuki. Persistent propagation of concentration waves in dissipative media far from thermal equilibrium. *Prog. Theor. Phys.*, 55:356–369, 1976.

[2] Yamada and Y. Kuramoto. A reduced model showing chemical turbulence. *Prog. Theor. Phys.*, 56:681, 1976.

[3] G. I. Sivashinsky. Nonlinear analysis of hydrodynamic instability in laminar flames i. derivation of basic equations. *Acta Astronaut.*, 4:1177–1206, 1977.

[4] G. I. Sivashinsky. On flame propagation under conditions of stoichiometry. *SIAM J. Appl. Math.*, 39(1):190–193, 1980.

[5] G. I. Sivashinsky and D. Michelson. On irregular wavy flow of a liquid film down a vertical plane. *Prog. Theor. Phys.*, 63:2112–2114, 1980.

[6] K. Kassner, A. K. Hobbs, and P. Metzener. Dynamical patterns in directional solidification. *Physica D.*, 93(23), 1996.
[7] Basil Nicolaenko, Bruno Scheurer, and Roger Temam. Some global dynamical properties of the Kuramoto-Sivashinsky equations: nonlinear stability and attractors. *Physica D: Nonlinear Phenomena*, 16(2):155–183, 1985.
[8] Pierre Collet, Jean-Pierre Eckmann, Henri Epstein, and Joachim Stubbe. A global attracting set for the Kuramoto-Sivashinsky equation. *Commun. Math. Phys.*, 152(1):203–214, 1993.
[9] Jonathan Goodman. Stability of the Kuramoto-Sivashinsky and related systems. *Commun. Pure Appl. Math.*, 47(3):293–306, 1994.
[10] Lorenzo Giacomelli and Felix Otto. New bounds for the Kuramoto-Sivashinsky equation. *Commun. Pure Appl. Math.*, 58(3):297–318, 2005.
[11] Jared C Bronski and Thomas N Gambill. Uncertainty estimates and L2 bounds for the Kuramoto-Sivashinsky equation. *Nonlinearity*, 19(9):2023, 2006.
[12] Felix Otto. Optimal bounds on the Kuramoto–Sivashinsky equation. *J. Funct. Anal.*, 257(7):2188–2245, 2009.
[13] Igor Kukavica and David Massatt. On the global existence for the kuramoto-sivashinsky equation. *Journal of Dynamics and Differential Equations*, pages 1–17, 2021.
[14] X. Yan and S. Chi-Wang. Local discontinuous Galerkin methods for the Kuramoto-Sivashinsky equations and the ito-type coupled KdV equations. *Comput. Methods Appl. Mech. Engrg.*, 195:3430–3447, 2006.
[15] A.H. Khater and R.S. Temsah. Numerical solutions of the generalized Kuramoto-Sivashinsky equation by Chebyshev spectral collocation methods. *Comp. Math. Appl.*, 56:1465–1472, 2008.
[16] M. Lakestani and M. Dehghan. Numerical solutions of the generalized Kuramoto-Sivashinsky equation using B-spline functions. *Appl. Math. Model.*, 36:605–617, 2012.
[17] S. Haq, N. Bibi, S.I.A. Tirmizi, and M. Usman. Meshless method of lines for the numerical solution of generalized Kuramoto-Sivashinsky equation. *Appl. Math. Comput.*, 217:2404–2413, 2010.
[18] E.J. Parkes and B.R. Duffy. An automated tanh-function method for finding solitary wave solutions to non-linear evolution equations. *Comput. Phys. Comm.*, 98:288, 1996.
[19] D. W. Peaceman and H. H. Rachford. The numerical solution of parabolic and elliptic differential equations. *J. Soc. Indust. Appl. Math.*, 3:28–42, 1955.
[20] J. Douglas and H. Rachford. On the numerical solution of heat conduction problem in two and three space variables. *Trans. Amer. Math. Soc.*, 82(2):421–439, 1956.
[21] G. I. Marchuk. Methods of numerical mathematics. *Springer Verlag*, 1982.
[22] R. J. LeVeque. Finite-volume methods for hyperbolic problems. *Cambridge University Press*, 2004.
[23] E. Tadmor and H. Nessyahu. Non-oscillatory central differencing for hyperbolic conservation laws. *J. Comput. Phys.*, 87:408–463, 1990.
[24] E. Tadmor and L. Xu-Dong. Third order nonoscillatory central scheme for hyperbolic conservation laws. *Num. Math.*, 79:397–425, 1998.

[25] K. Alexander and E. Tadmor. New high-resolution central schemes for nonlinear conservation laws and convection-diffusion equations. *J. Comput. Phys.*, 160:241–282, 2000.

[26] K. Alexander, N. Sebastian, and P. Guergana. Semidiscrete central-upwind schemes for hyperbolic conservation laws and Hamilton-Jacobi equations. *SIAM. J. Sci. Comput.*, 23(3):707–740, 2001.

[27] K. Yong-Jung, H. Youngsoo, and T. G. Myers. On the numerical solution of a driven thin film equation. *J. Comput. Phys.*, 227:7246–7263, 2008.

[28] Denis Anders, Maik Dittmann, and Kerstin Weinberg. A higher-order finite element approach to the Kuramoto-Sivashinsky equation. *J. Appl. Math. Mech.*, 92(8):599–607, 2012.

[29] A. P. Hooper and R. Grimshaw. Traveling wave solutions of the Kuramoto-Sivashinsky equation. *Wave Motion*, 10:405–420, 1988.

[30] D. Michelson. Steady solutions of the Kuramoto-Sivashinsky equation. *Physica 19D*, pages 89–111, 1986.

[31] J. Nickel. Travelling wave solutions to the Kuramoto-Sivashinsky equation. *Chaos Soliton. Fract.*, 33:1376–1382, 2007.

[32] Milena Stanislavova and Atanas Stefanov. Asymptotic estimates and stability analysis of Kuramoto-Sivashinsky type models. *J. Evol. Equ.*, 11(3):605–635, 2011.

[33] P Veeresha and DG Prakasha. Solution for fractional kuramoto–sivashinsky equation using novel computational technique. *International Journal of Applied and Computational Mathematics*, 7(2):1–22, 2021.

[1]Department of Mathematics and Applied Mathematics, University of Pretoria, Pretoria 0002, South Africa

[2]Department of Mathematics, Obafemi Awolowo University, Ile-Ife, Nigeria